ORIGINAL ARTICLE

In vitro corrosion resistance and cytocompatibility of minerals substituted apatite/biopolymers duplex coatings on anodized Ti for orthopedic implant applications

A. Sasireka, Renji Rajendran, V. Raj *

Advanced Materials Research Laboratory, Department of Chemistry, Periyar University, Salem 636 011, Tamil Nadu, India

Abstract In this work, strategies for the formation of duplex coatings with enhanced bioactivity, mechanical properties and corrosion resistance have been focused. TiO_2 arrays were fabricated on Ti alloy were carried out in a single step using suitable electrolyte by anodization method. Here, we have synthesized a novel bioactive material, minerals incorporated Hydroxyapatite (La/Tb-HAP)-chitosan-casein duplex coatings on anodized Ti via electrodeposition method. The fabricated novel composite coatings were characterized by FT-IR, XRD, FESEM and EDAX analyses. Also, the mechanical properties of duplex coatings were scrutinized by Dermitron thickness and microhardness tester. The corrosion resistance of the as-developed duplex coatings was studied by electrochemical techniques using Ringers solution as the electrolyte. In addition, the antibacterial activity, cell viability, live and dead staining were executed to substantiate the biocompatibility of TNT/CS-CA@M-HAP duplex coatings. From the overall summary of this work, it is proved that the resultant CS-CA@M-HAP coatings on TNT exhibit excellent bioactivity and improved corrosion resistance over pure Ti and serve as a potential candidate for orthopedic applications.
© 2020 Published by Elsevier B.V. on behalf of King Saud University. This is an open access article under the CC BY-NC-ND license (http://creativecommons.org/licenses/by-nc-nd/4.0/).

1. Introduction

In this field of materials science and implantology researchers have been looking for improvements in the design of devices useful for clinical applications in body part replacement. Bone has been one of the crucial target-tissues, because of its specific properties and the possibility to tackle its functional repair using rigid biocompatible implants and surgical techniques (Civantos et al., 2017).

* Corresponding author.
  E-mail address: alaguraj2@rediffmail.com (V. Raj).
Peer review under responsibility of King Saud University.

Production and hosting by Elsevier

At present, titanium (Ti) and its alloys are extensively used as biomedical application for the conception of long-term prosthetic heart valves including artificial hip joint replacement, orthodontic, interventional cardiovascular stents and orthopedic implants compared to stainless steel and magnesium alloys, mainly due to the combination of their outstanding mechanical strength, high corrosion resistance and good biocompatibility (Saini, 2015). However, Ti based implants suffer some shortcomings; the material has bioinert in nature and lack of osseointegration, that cannot form an effective bone-bonding ability between the host tissue and the implant, which may cause the failure of implant (Agarwal et al., 2016). To overcome these limitations, it is necessary to apply a suitable surface treatment (Bai et al., 2018) on Ti implants to improve the bone- bonding ability.

Traditional Ti implants were produced by processing Titanium nanotubes followed by further surface modification, such as chemical deposition, sol-gel dipping (Lotz et al., 2018), laser deposition (Metoki et al., 2014), plasma-induced grafting (Kumar et al., 2014), anodic oxidation (Poverenov et al., 2014), electrophoretic deposition (Poverenov et al., 2014) have been explored to improve stability and enhance osseointegration (Pogrebjak et al., 2016).

Hydroxyapatite (denoted as HAP) frequently used as bone/teeth implantations, bone fracture repairs, because its high chemical similarities with the biological calcified tissues make it very excellent bioactivity and biocompatibility (Kurek et al., 2014). Recently, this material has been also investigated for artificial bone substitute, gene or drug delivery, biological imaging, proteins and various drugs because of their high capacity to accept ionic substitutions. For instance, the advantages of doping HA with foreign ions such as Ag^+, Sr^{2+}, Mg^{2+}, Mn^{2+}, Ce^{3+}, Sm^{3+}, etc for orthopedic applications were reported by others.

Recently, a novel multifunctional nanostructure of La^{3+}, Tb^{3+} co-doped HAP used to detect the fluorescent labelling of the biological interactions and magnetic properties during implantation have been reported (Chen et al., 2016). It can be noted that the higher content of La^{3+} ions included with HAP may leads to a better antibacterial effect but it can also upsurge the cytotoxicity. To reduce the toxicity, the secondary material can be introduced with good bioactivity.

Tb^{3+} ion has a functional mimic of the Ca^{2+} ions that can affect the regeneration and remodeling of bone and it is used for the disorderness of bone density treatment such as osteoporosis, osteomyelitis, etc.

One of the limitations of M-HAP coatings on Ti implant material is leach out of toxic metal ions through pores into the tissues. Furthermore, it is reported that the adhesion between the coating of HAP and Ti is very poor. One of the important strategies used to generate more protective and adherent interfaces include the use of polymers. Natural biopolymer of Chitosan (CS) is recommended as a suitable functional material, because of its excellent biodegradability, biocompatibility, nontoxicity, high-quality film forming properties and low cost (Qin et al., 2015). To improve its mechanical strength, impregnation of rigid polymers likes gelatin (Manab, 2017), collagen (Azhar et al., 2014) and casein (Biranje et al., 2019) have also been included.

Casein is one of the most promising protein, an inexpensive, easily available, non-toxic, biocompatible and biodegradable material (Das et al., 2010). Casein is derived from phosphoproteins with the electronegative domains in casein micelles, more preferentially located in small fragments of peptide bonds. Casein has strongly acidic peptide of 40 amino acids that contains 7 of the 8 phosphate groups, 12 carboxyl groups and only four positive groups. Casein is the excellent source of Ca^{2+} ions and functional groups such as ─COOH, ─NH_2 and ─OH groups (Biranje et al., 2019; Hamedi et al., 2010). Casein is a negatively charged at pH 10, it can make strong interaction through hydrogen bonding with hydroxyl group and amino groups of chitosan, leading to better attraction between the polymers. Amine groups of chitosan are mostly protonated to NH_3^+ in acidic pH, and the resultant polysaccharide is positively charged. Casein also acquires a net positive charge, since the isoelectric point is 4.6–4.8, leading to electrostatic repulsion between the two polymer chains. In previous reports, chitosan (polysaccharide) can interact with casein (protein) to form either soluble or insoluble complexes, which is due to formation of coacervation depending on the pH (i.e. electrostatic interactions) (Devi et al., 2016).

To the best of author knowledge, this is the first time that the M-HAP/CS-CA/TiO_2 nanocomposite coatings have been prepared by the electrophoretic deposition and anodization method for biomedical applications. In these coatings, the microstructure and surface morphology were investigated by various techniques such as FT-IR, XRD, HRSEM and EDAX analyses. The mechanical properties of these coatings were evaluated by using thickness, Vickers micro-hardness and adhesion tests. The release of metal ions from the coatings was studied by inductively coupled plasma atomic emission spectroscopy (ICP-AES). In addition, the antibacterial property of the coatings was evaluated against G^+ ve bacteria and G^- ve bacteria. Then, the EIS spectra as well as Tafel curves were recorded with an electrochemical workstation to assess the in vitro anticorrosion behavior of the developed coatings in Ringers solution. Moreover, the in vitro osteocompatibility and cell proliferation of live/dead staining of MG-63 human osteoblast cells were tested for the resultant coatings. Finally, all the results displayed that the M-HAP/CS-CA/TiO_2 duplex layer coated Ti specimen can be potential for orthopedic applications with enhanced corrosion protection performance and improved mechanical and biological properties.

2. Materials and methods

Chitosan (Molecular weight in the range 550,000 g/mol, 90% Deacetylation), β-casein powder, acetic acid, ammonium fluoride, ammonium dihydrogen phosphate ($NH_4H_2PO_4$) and other chemicals were purchased from Merck used in analytical grade throughout the experiments without no further purification.

For M-HA electrolyte, calcium chloride dihydrate ($CaCl_2$·$2H_2O$, 99.9% purity, Sigma Aldrich, USA), lanthanum nitrate hexahydrate (La (NO_3)$_3$·$6H_2O$, 99.9% purity, Sigma Aldrich, USA), terbium nitrate pentahydrate (Tb (NO_3)$_3$·$5H_2O$, 99.9% purity, Sigma Aldrich, USA), were dissolved separately in deionized water. Diammonium hydrogen phosphate ($(NH_4)_2HPO_4$), isopropanol, absolute ethanol, ammonia purchased from (99% purity, Merck, India) were used as starting precursors. Development of various coatings was employed using electrosynthesized polymer blended solutions coated on

M-HAP, and the whole experimental section was performed at room temperature. Deionized water and ethanol were used in the preparation of all the aqueous electrolytes.

2.1. Preparation of TNT coatings on RBA

The commercially pure Ti sheets were procured from Sigma-Aldrich Chemie, GmbH, Schnell dorf, Germany. The Ti substrates were cut into dimensions of $10 \times 10 \times 0.5$ mm^3. Prior to the anodization process, the working electrode (Ti) substrates of 1 cm^2 surface were mechanically grounded with silicon carbide sheets of different grade size ranging from 400 to 1200 grits. These metallic Ti substrates were thoroughly washed in 1:1 ratio of ethanol/acetone mixture in an ultrasonic bath, followed by polishing solution containing HF, HNO$_3$, and H$_2$O with a volume ratio 1:4:5 for 5 min at room temperature to remove unwanted impurities and then rinsed with distilled water, dried in air for improved the coating adhesion onto the substrate. After chemical polishing, the anodization was performed in a two electrode cell connected to a DC power supply using Ti substrate as the anode and graphite as cathode at 40 V for 60 min in an electrolyte containing 0.5 wt% NH$_4$F and 1 M NH$_4$H$_2$PO$_4$ under thermostatically controlled manner. After anodization, TiO$_2$ formed on Ti substrates were washed with tap water and dried by annealing at 450 °C for 2 h.

2.2. Synthesis of polymers coatings on TiO$_2$ substrate.

1 g of chitosan was dissolved in 1% acetic acid containing 100 ml of water, and the prepared CS solution was stirred overnight to form clear solution. To prepare a casein solution at various concentrations, 1%, 2%, and 3% of casein powder prepared separately by adding 1 M NaOH solution was stirred and clear solution was obtained by maintaining at pH 10.

Briefly, 50 ml of 1% (w/v) chitosan solution and 50 ml of casein solutions at various concentrations were mixed together and stirred for 3 h. The electrophoretic deposition of polymer blends on TiO$_2$ substrate was carried out by using a DC power supply kept at a constant potential 2 V with a deposition time of 45 min.

2.3. Electrodeposition of M-HAP on chitosan-casein coated TiO$_2$ substrate.

The electrodeposition of M-HAP on CS-CA/TNT coated Ti specimen was performed potentiostatically by using an electrochemical workstation (CHI 760C, CH Instruments, USA) at constant current density of 9 mA cM-^{2} for 30 min). Three categories of M-HA electrolytes were utilized for the development of M-HAP.

Category 1 M-HAP (I): 0.4 M CaCl$_2$·2H$_2$O, 0.05 M La (NO$_3$)$_3$·6H$_2$O, 0.05 M Tb(NO$_3$)$_3$·6H$_2$O and 0.3 M (NH$_4$)$_2$HPO$_4$.

Category 2 M-HAP (II): 0.375 M CaCl$_2$·2H$_2$O, 0.05 M La (NO$_3$)$_3$·6H$_2$O, 0.075 M Tb(NO$_3$)$_3$·6H$_2$O and 0.3 M (NH$_4$)$_2$HPO$_4$.

Category 3 M-HAP (III): 0.375 M CaCl$_2$·2H$_2$O, 0.05 M La (NO$_3$)$_3$·6H$_2$O, 0.1 M Tb(NO$_3$)$_3$·6H$_2$O and 0.3 M(NH$_4$)$_2$HPO$_4$.

The above solutions were prepared to produce the target molar ratio of (Ca + La + Tb)/P as 1.67. After that time, slowly anionic solution was added dropwise to cationic solution and pH of the electrolyte was adjusted to 10.0 by using NH$_4$OH solution. During the deposition process, minerals substituted HA electrolyte was deaerated with N$_2$ atmosphere for 30 min, in order to reduce the formation of calcium carbonate (CaCO$_3$) deposits and thus to diminish the carbon dioxide (CO$_2$).

The deposition process of TNT/CS-CA@M-HAP (I) to TNT/CS-CA@M-HAP (III) coated on Ti substrate were carried out from all the above three categories of the solutions under magnetic stirring for 5 h, then the coating on Ti specimen were rinsed with deionized water and then dried for overnight at room temperature.

2.4. Characterization of TNT/CS-CA @M-HAP duplex coatings on Ti substrates

The Fourier Transform- infrared spectroscopy (FT-IR, Perkin Elmer RX1 Spectrometer) was used to confirm the functional groups of the as-formed TNT, TNT/CS-CA, TNT/CS-CA@M-HAP-I, TNT/CS-CA@M-HAP-II and TNT/CS-CA@M-HAP-III duplex coatings on Ti substrates in the reflectance absorption mode in the range 4000–400 cm^{-1}. The coatings samples scraped from the surface of Ti were mixed with KBr were pressed into discs and made them into pellet form and then analyzed.

The phase identification and crystallinity of the TNT/CS-CA@M-HAP nanocomposite samples were analyzed by XRD experiments using PANalytical X' Pert PRO diffractometer with monochromatic CuKα radiation (1.5406 Å) generated at 40 kV and 30 mA in the range between $20° \leq 2\theta \leq 80°$ with a scan rate of 0.02° at a scanning angle of 10 min^{-1}, respectively by comparing the XRD patterns with standard data compiled by the JCPDS software. The average crystallite size of the synthesized samples were determined using the Debye-Scherrer approximation (Sasireka et al., 2019).

$$D = K\lambda/(\beta cos\theta)$$

where D is the average crystallite size calculated for the (hkl) reflectance, λ is the wavelength of radiation (λ = 1.5406°) in A°, β is the full width at half maximum approximation (FWHM) in radian, θ is the angle of diffraction as represented in degrees and K is the broadening constant.

To investigate the morphological structure of the samples (TNT, TNT/CS-CA, TNT/CS-CA@M-HAP-I, TNT/CS-CA@M-HAP-II and TNT/CS-CA@M-HAP-III duplex layer coated on Ti were scrutinized by using high resolution scanning electron microscope (HRSEM, JEOL, JSM-840A) and cross- sectional analysis of all coated samples was also carried out. Before handling HRSEM analysis, the specimens were coated by gold sputtering and all coated samples were recorded using the secondary electron detectors. The elemental composition and elemental mapping of the deposited duplex layer coatings on Ti was investigated by using an energy dispersive X-ray (EDAX) analysis. The coated specimens were immersed in fresh Ringer's solution for 1 h to leach out mineral ions characteristics of the TNT, TNT/CS-CA, TNT/CS-CA@M-HAP-I, TNT/CS-CA@M-HAP-II and TNT/CS-CA@M-HAP-III duplex coatings on Ti and they were evaluated using the inductively coupled plasma atomic emission spectroscopy (ICP-AES, Instruments, Wrexham, UK).

2.5. Mechanical properties of the coatings

2.5.1. Adhesion strength

The adhesion strength can present most valuable information about the mechanical properties of the duplex layer coating and that is the most vital property for in vivo implantation. The TNT/CS-CA@M-HAP duplex layer coated on Ti specimens were evaluated for the adhesion strength by pull-out test according to the American Society for Testing Materials (ASTM) international standard F1044-05. Each experiment was repeated at least five times for all coated samples cured in an oven at 100 °C for 50 °C and the average was taken. The specimens were exposed to pull-out tests using a universal testing Machine (model 5569, Instron Co., USA) at a constant crosshead speed of 1 mm min^{-1}.

2.5.2. Thickness and micro hardness

The Dermitron thickness tester was used to measure thickness of coating in more than three different places in the specimen and taken the average value. Vickers microhardness measurements were performed on the TNT, TNT/CS-CA, TNT/CS-CA@M-HAP (I), TNT/CS-CA@M-HAP (II) and TNT/CS-CA@M-HAP (III) duplex layer coated Ti substrate, respectively using an Automatic HV-1000B series hardness tester (Sasireka et al., 2019). The load used was 490.3mN and the cross-sectional micro hardness values were measured with 25 g load for a dwell time of 30 s. The micro hardness (HV) value was calculated for each coating sample by subjecting to at least five measurements under the same testing and the average was taken.

2.6. Antibacterial activity

The antibacterial activity of the TNT/CS-CA@M-HAP (II) duplex layer coated on Ti substrate have been tested against two prokaryotic strains *S. aureus* (ATCC 25923) and *E. coli* (ATCC 25922) using agar well diffusion technique, in performed at Muller-Hinton agar plates by pouring agar for thick dense layers and adding inoculated of the test microorganisms of two bacterial strains via. Gram positive bacteria and Gram negative bacteria and then incubated at 37 °C for overnight in Trypticase Soy Broth (TSB) cultures to obtain better growth. Petri discs of 6 mm diameter were left for 10 min in the laminar flow and were immersed into various concentrations (25, 50, 75, 100 µL) of different samples (Pishbin et al., 2014). The antibacterial activity was evaluated by measuring the zone of inhibition around the disc produced by the coating samples against the two bacterial strains.

2.7. Invitro biological studies

2.7.1. Cell viability

The cell viability of TNT/CS-CA@M-HAP composites was tested on MG-63 osteoblast cells supplied by National Centre for Cell Sciences (NCCS), Pune, India. The viability of cells colonizing the samples was performed using a modified MTT (3-(4,5-dimethyl-2-thiazolyl)-2,5-diphenyl tetrazolium bromide) assay. Cells at a density of 1×10^5 cells/well were seeded onto a 24 well plates maintained in a humidified 5% CO_2 atmosphere and incubated overnight at 37 °C $\pm$ 1 °C. The cul-

ture media was replaced with fresh medium every day and the cells were subcultured by trypsinization. After being incubated for 1 day, 4 days and 7 days, the samples TNT/CS-CA@M-HAP substrate were removed from the respective wells, washed three times with phosphate-buffered saline (p^H = 7.4) [PBS, OXOID Limited, England] solution prior to any toxicity assays. Only those cells that are adherent to the well walls were found viable and incubated with 0.5% 3-[4,5-dimethylthiozol-2-yl]-2,5-diphenyl tetrazolium bromide [MTT] solution was detached. The viable cells reduce the MTT into insoluble formazan precipitate by mitochondrial succinic dehydrogenase (Jadalannagari et al., 2014). After incubation for 4 h, 0.1% dimethyl sulfoxide (DMSO) was added to each well for dissolving the formazon crystals and the absorbance values were measured in an Enzyme- Linked Immunosorbent Assay (ELISA) microplate (SPR-960) at λmax of 570 nm, and the percentage of cell viability were measured with respect to control at 1 day, 4 days and 7 days of the TNT/CS-CA@M-HAP (at optimum concentration) duplex layer coated on Ti substrate was calculated from the average five replicates using the following formula:

$$(\%) Cell\ viability = \frac{[A]test}{[A]control} \times 100$$

2.7.2. Live and dead staining

After cell culture, the coated TNT/CS-CA@M-HA (III) samples were stained using live/dead assay. Every time, the DMEM media was discarded and the samples were washed with PBS solution, the live/dead stained solution containing 50 µL of 1 mg/ml acridine orange and ethidium bromide were added to individual well, mixed gently, and were incubated at 37 °C at 5% CO_2 incubator for 24 h. After incubation, the stain were viewed using fluorescence microscope (Kolanthai et al., 2015).

2.8. Electrochemical evaluation of composite coatings on Ti

The corrosion resistivity of uncoated Ti and TNT/CS-CA, TNT/CS-CA@M-HAP (I), TNT/CS-CA@M-HAP (II), TNT/CS-CA@M-HAP (III) (at optimum concentration of La^{3+}, Tb^{3+}) duplex coated on Ti specimens was determined by Tafel polarization and Electrochemical impedance spectroscopy (EIS) in Ringer's solution (with composition 8.6 g/l NaCl; 0.66 g/l $CaCl_2 \cdot 2H_2O$ and 0.6 g/l KCl) at pH 7.4 and commonly accepted human body temperature, 37 $\pm$ 1 °C. Generally, the electrochemical corrosion experiments were done in the three-electrode system using the electrochemical workstation model CHI 760 (CH INSTRUMENTS, USA) with platinum and saturated calomel electrode (SCE) as counter and reference electrodes, respectively. The coated Ti specimens were used as the working electrodes of dimension 1 cm^2 area and its corrosion potential was measured related to SCE. Before the electrochemical studies, working electrodes were allowed to become stable until it reached a steady potential denoted as the open circuit potential (OCP).

The potentiodynamic polarization experiments were performed as the potential range from −0.4 V to + 1.2 V vs SCE for uncoated Ti and TNT/CS-CA, TNT/CS-CA@M-HAP (I), TNT/CS-CA@M-HAP (II), TNT/CS-CA@M-HAP (III) duplex coated samples on Ti at a sweep rate of

1.0 mV s^{-1}. During the cyclic polarization studies, the potential was raised in noble direction, until the breakdown potential (E_b) was reached. The breakdown potential (E_b) was obtained at the potential where there was a monotonic raise in the current density. The repassivation potential (E_{pp}), is one at which the scan meets reverse the passive region. Likewise, the electrochemical impedance spectra (EIS) were recorded over the frequency ranging from 10^{-1} Hz to 10^5 Hz and with applied AC perturbation amplitude of 5 mV. To confirm the reproducibility, all electrochemical experiments were repeated at least three times and the obtained data was recorded using the internally available software.

3. Results and discussion

3.1. Functional group analysis

Representative Fourier Transform infrared (FTIR) spectra have been used for determining functional groups or chemical bonds that exist in a material. Fig. 1 (a-e) illustrates the FTIR spectra of anodized Ti, CS and CA blending on TNT and M-HAP (M-La^{3+}, Tb^{3+}) deposited on CS-CA/Titania nanotubes and under at various concentrations of trivalent ions. From Fig. 1a, it can be observed that the peaks at 3429 cm^{-1} and 2990 cm^{-1} are attributed to the O-H stretching vibration modes of water molecule adsorbed on the surface and bending vibrations of OH groups respectively. This indicates that a sig-
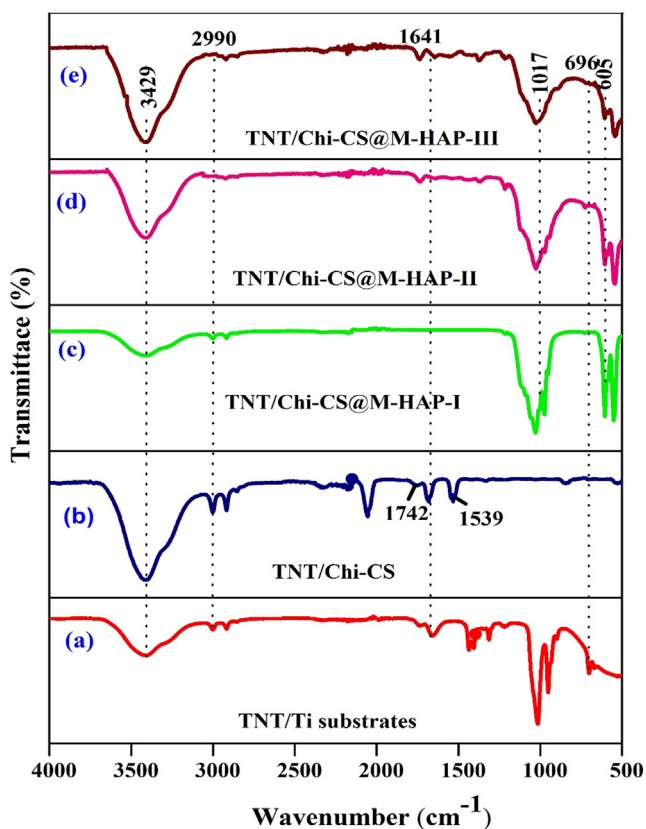
Fig. 1 FT-IR spectra of (a) TNT (b) TNT/CS-CA (c) TNT/CS-CA@ M-HAP (I) (d) TNT/CS-CA@ M-HAP (II) (e) TNT/CS-CA@ M-HAP (III) coatings on Ti substrate.

nificant fraction of H$_2$O and OH groups exist in as anodized sample and intensity of peak is very low due to annealing. The bands at 696 cm^{-1} and 540 cm^{-1} are assigned to the vibration of Ti-O and Ti-O-Ti bond in TNT (Mohan Raj et al., 2018).

Fig. 1b shows the sequential binary coatings with chitosan (CS) and casein (CA) coated on TNT. It shows strong IR absorption bands at 3440 cm^{-1} and 1742 cm^{-1} corresponds to –OH stretching vibration and amino group of chitosan that are shifted to 1609, 1539 and 1220 cm^{-1} that arise from N-H stretching and amide bending vibration bands and peak at 1641 cm^{-1} is due to C=O stretching vibration of casein (Singh et al., 2015).

Fig. 1(c–e) shows that the FT-IR spectra of M-HAP characteristic vibrations of phosphate groups occurs at 1017 cm^{-1} and 605 cm^{-1} respectively. The broad band of stretching vibration modes of OH groups can be located at 3429 cm^{-1}, due to presence of hydrogen bonded water molecule absorbed during apatite formation (Farzadi et al., 2014, Chang et al., 2013). The sharp peak indicates two stretching vibration modes of La-OH and Tb-OH at 653 cm^{-1} and 720 cm^{-1} present in M-HAP composite coating respectively (Hosseini et al., 2014).

3.2. Phase identification and structure

Fig. 2(a–e) shows the XRD patterns of TNT, TNT/CS-CA, TNT/CS-CA@M-HAP (I), TNT/CS-CA@M-HAP (II) and TNT/CS-CA@M-HAP (III) duplex layer coatings fabricated on Ti alloy. Fig. 2(a) illustrates the XRD pattern of TNT which shows diffraction peaks with planes at 2θ positions of 25.2° (1 0 1), 37.9° (1 0 3), 48.6° (2 0 0), 53.8°(1 0 5), 63.7° (2 1 3), 75.3° (1 0 7) that corresponds to anatase form of TiO$_2$ (JCPDS card no: 21–1272). The very sharp peak of anatase phases of titania formed during anodization indicate the highly crystalline nature of the coating (Raj and Mohan Raj, 2016).

The strong interaction was observed between with addition of chitosan and casein molecules as those of mechanical blending. XRD pattern of TNT/CS-CA composite coating depicted in Fig. 2b shows the new diffraction peaks at 2θ values of 12.6°, 18.5° are assigned to CS, CA composite coating, respectively and the results are in accordance with the earlier reports (Surmeneva et al., 2013). The high crystallinity is appeared due to the strong interaction of chitosan with casein through hydrogen bonding between hydroxyl groups and amine groups.

The XRD patterns for M-HAP coatings on TiO$_2$/CS-CA substrates show similar diffraction peaks representing the HAP formation which indicates that all coated samples exhibit a similar crystallographic nature as depicted in Fig. 2(c–e). The peaks of M-HAP correspond to the 2θ values of 25.8°, 27.2°, 30.4°, 31.9°, 32.5° and 35.9° without any secondary phases are found.

XRD peaks identified for M-HAP well match with the standard XRD data (JCPDS No: 09-0432, JCPDS No: 01-083-2038). However, the 2θ values for M-HAP peak positions are shifted towards the lower angles which might have aroused due to influence of the lanthanum and terbium mineral ions substitution that leads to the distortion in the HAP lattice (Sohn, 2014, Stancheva and Bojinov, 2012). This could be recognized due to the presence of M-HAP in the duplex coatings.
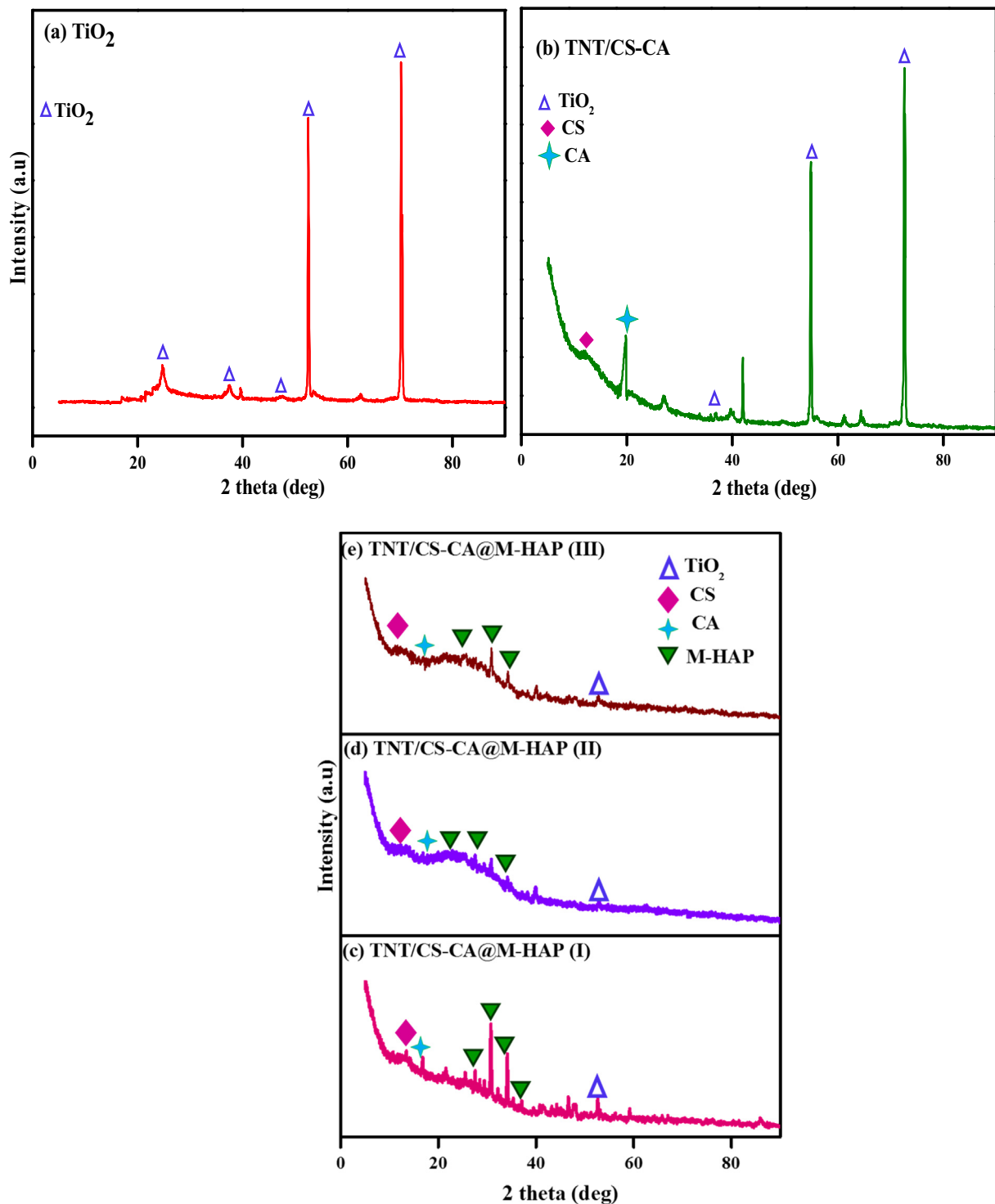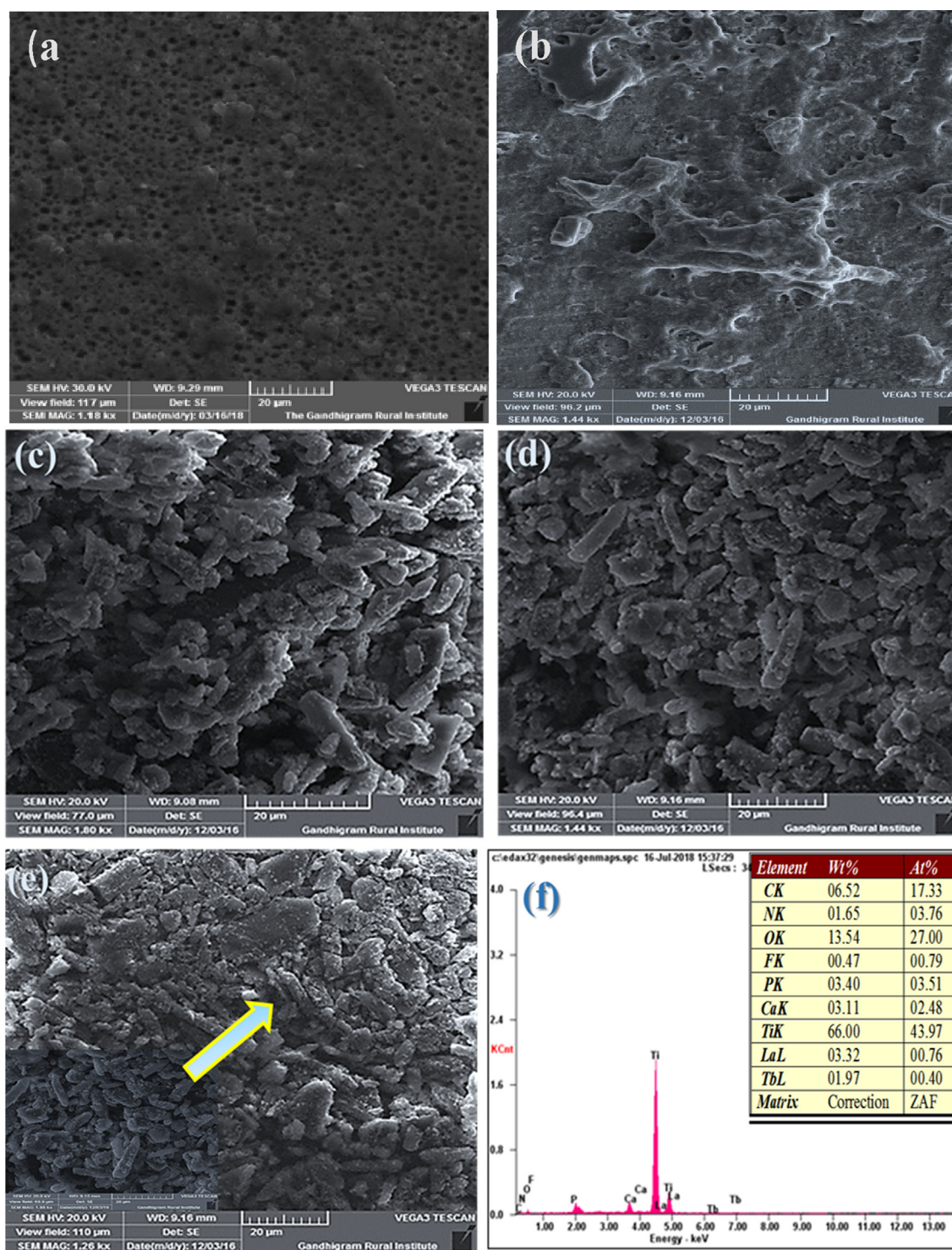
Fig. 2 XRD spectra of (a) TNT (b) TNT/CS-CA (c) TNT/CS-CA@ M-HAP (I) (d) TNT/CS-CA@ M-HAP (II) (e) TNT/CS-CA@ M-HAP (III) coatings on Ti substrate.

3.3. Morphological observation

Fig. 3a depicts SEM images of highly ordered close packed titania nanotube arrays after annealing at 450 °C for 3 h prepared by electrochemical anodization of Ti using the 1 M $(NH_4)_2HPO_4$ + 0.5% NH_4F electrolyte solution for 90 min at 40 V. The SEM top-view image (Fig. 3a) reveals a wide distribution of average diameter of 20 nm pores. In these experiments, the fluoride concentration was varied from 0.5 to 2 wt %. Indeed, that source of fluoride is typically water soluble and more ionic nature. Therefore, an increase in fluoride concentration yields an increase in overall ionic concentration of the solution which results in an increase in electrolyte conductivity and higher current response. The fluoride ions are more

Element	Wt%	At%
CK	06.52	17.33
NK	01.65	03.76
OK	13.54	27.00
FK	00.47	00.79
PK	03.40	03.51
CaK	03.11	02.48
TiK	66.00	43.97
LaL	03.32	00.76
TbL	01.97	00.40
Matrix	Correction	ZAF

Fig. 3 HRSEM micrographs of (a) TNT (b) TNT/CS-CA (c) TNT/CS-CA@ M-HAP (I) (d) TNT/CS-CA@M-HAP (II) (e) TNT/CS-CA@ M-HAP (III) coatings on Ti substrate (f) EDAX spectrum of the TNT/CS-CA@ M-HAP (II) coating.

rich species in these electrolytes that can be assumed to be prone to chemical dissolution in aqueous environment (Lee et al., 2009).

Fig. 3b demonstrates the morphology of coatings (CS-CA) that exhibit less porous structure. The phase separation of polymeric hydrogel synthesized using CS-CA has lesser porosity with various irregular segregated structures as shown in

Fig. 3b. In this study, the polymer adhere onto TNT were used to enhance the number of pores and pore size was decreased which might be due to significant formation of tightly packed network structure. The embedding of this polymer resulted in apparently reduction in pore size (Govindaraj et al., 2015).

The structural morphologies of the electrodeposited of M-HAP-I, M-HAP-II and M-HAP-III coatings on CS-CA/TNT

composite coating samples are depicted in Fig. 3c-e. The M-HAP-I (Fig. 3(c)) coating is heterogeneous with agglomerated granules over the surface. Similarly, the M-HA-II coating (Fig. 3(d)) and M-HAP-III coating (Fig. 3(e)) exhibit the interconnected granular structure, but Fig. 3d exhibits uniform coverage of interconnected granular structure and the small pores that exist in the coating is taken as optimum condition for good anticorrosion and improved cell attachment. In Fig. 3 (f) shows the EDS spectrum of TNT/CS-CA@M-HAP coated surfaces which shows Ca, P, C, O, Ti, La and Tb elements and the spectrum supports for the presence of trivalent ions of the as-developed coating.

Fig. S1 shows the elemental mapping of TNT/CS-CA@M-HAP(II) composite coating indicating the ubiquitous presence of Ca, P, C, O, Ti, La and Tb elements. Thus, the homogeneously distributed mineral ion is well evidenced from the EDS mapping results.

3.4. Leach out analysis

The release of mineral ions from the TNT/CS-CA@M-HAP (II) composite coated Ti was evaluated from the ICP-AES analysis after soaking in Ringer's solution for 1, 4 and 7 days and the results are shown in Fig. 4. The average Ca and P ion concentration ions released in the solution increased at day 1. Likewise, the release of other minerals such as La and Tb ions in the solution also slightly increased as increase immersion time from 0 to 1 day. Moreover, as the immersion time increases from 4 to 7 days, the release of mineral ions slightly decreased, which may be due to formation of apatite growth on the surface of the coating. From the resultant coatings, the released mineral ions such as Ca, P, La and Tb will be effectively take part in the antibacterial and bioactive properties. (Sasireka et al., 2019; Sohn, 2014; Devi et al., 2016).

3.5. Thickness, hardness and adhesion strength

Figs. 5 and 6 shows the thickness, hardness and adhesion strength values of Ti alloy, TNT, TNT/CS-CA, TNT/CS-
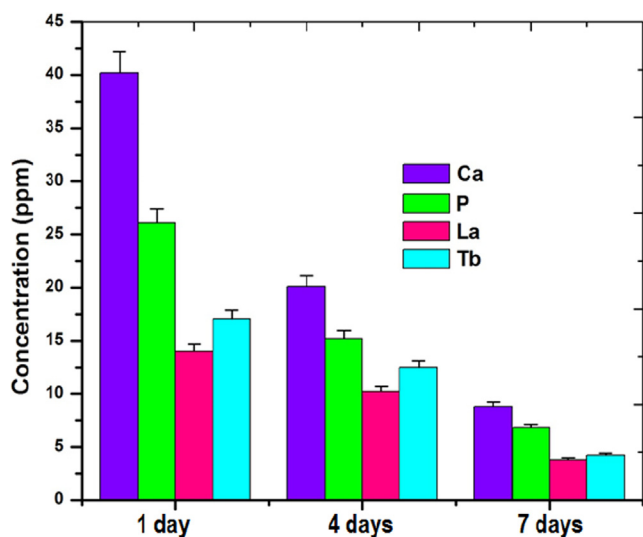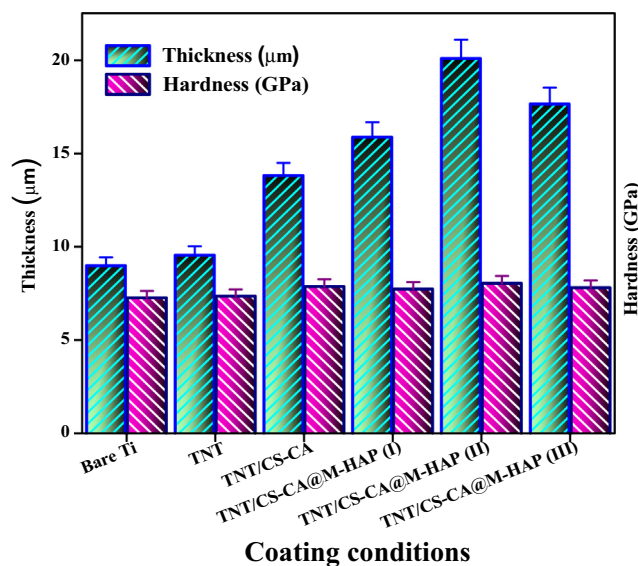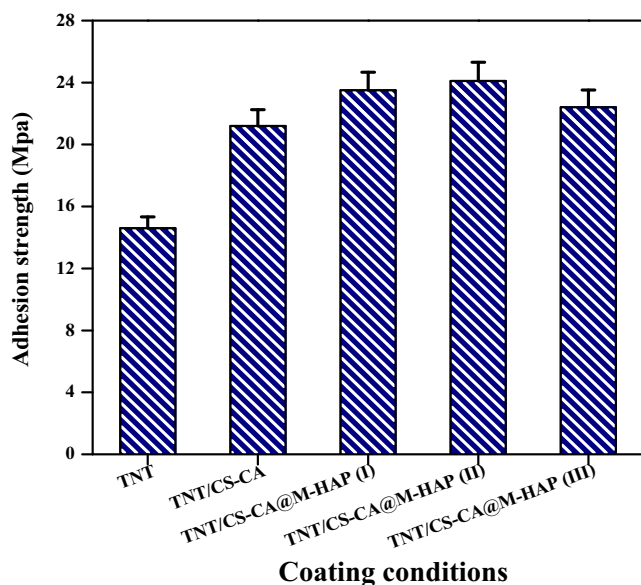

Fig. 5 Thickness, Hardness of various coated samples on Ti specimen.

CA@M-HAP (I), TNT/CS-CA@M-HAP (II) and TNT/CS-CA@M-HAP (III) composite coatings. The mechanical properties of TNT arrays such as thickness, hardness and adhesion strength were almost same when compared to the Ti substrate and these values increased when CS-CA was coated on TNT and it is further increased for TNT/CS-CA@M-HAP (II) composite coating. Thus TNT/CS-CA@M-HAP (II) coating shows maximum thickness, hardness and adhesion strength than any other coatings.

In this particular case, presence of CS-CA allowed good mixing of TNT, CS-CA, La, Tb and HAP layers by modifying their respective surface charges, thereby permitting the formation of uniform multi layers on Ti substrate enabling good mechanical strength to the substrate. Due to the presence of these multi layers, the overall thickness of the coating is higher which obviously increase the mechanical properties of the coatings. In the same manner, the mechanical properties of the coating and thickness are high for TNT/CS-CA@M-HAP (II) coating compared to other coatings but adhesion strength remains the same. This could be due to decrease in the porosity of the coatings as the addition of minerals increases.
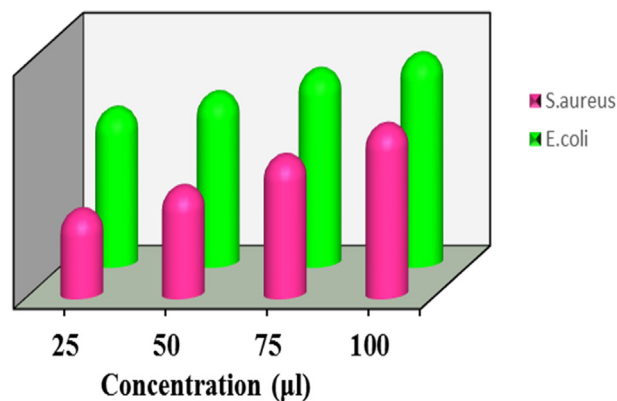
3.6. Antibacterial activity

The antibacterial activity of as-synthesized TNT/CS-CA, TNT/CS-CA@M-HAP (I), TNT/CS-CA@M-HAP (II) and TNT/CS-CA@M-HAP (III) composite coatings was studied and the zone of inhibition at four different concentration such as 25 μL, 50 μL, 75 μL and 100 μL against the pathogenic bacteria, namely $S.$ $aureus$ (G$^+$) and $E.$ $coli$ (G$^-$) by the disc diffusion method and depicted in Figs. 7 and 8. These data revealed, the substitution of La^{3+} and Tb^{3+} minerals in the HAP concentration in the coating. The zone of inhibition for the TNT/CS-CA@M-HAP (II) sample against $S.$ $aureus$ and $E.$ $coli$ were found to be 11 & 20 mm for 25 μL, 14 & 22 mm for 50 μL, 18 & 25 mm for 75 μL and 22 & 27 mm for 100 μL concentrations, respectively. At 100 μL, the TNT/

Fig. 4 ICP-AES analysis of TNT/CS-CA@ M-HAP (II) bilayer coated on Ti samples at different immersion days.

Fig. 6 Adhesion strength of various coated samples on Ti specimen.

CS-CA@M-HAP (II) duplex layer sample recorded superior antibacterial activity against *E. coli* by exhibiting the highest diameter of inhibition zone (Pogrebnjak et al., 2019). The antibacterial activity of TNT/CS-CA@M-HAP (II) duplex layer coatings against *E. coli* strain was slightly higher than that of *S. aureus* strain due to the differences observed in the structure of cell wall. The reason may be ascribed to the substitution of minerals such as La^{3+} and Tb^{3+} in HAP and also polymer composite incorporation in TNT plays a very important role in enhancing the antibacterial activity.
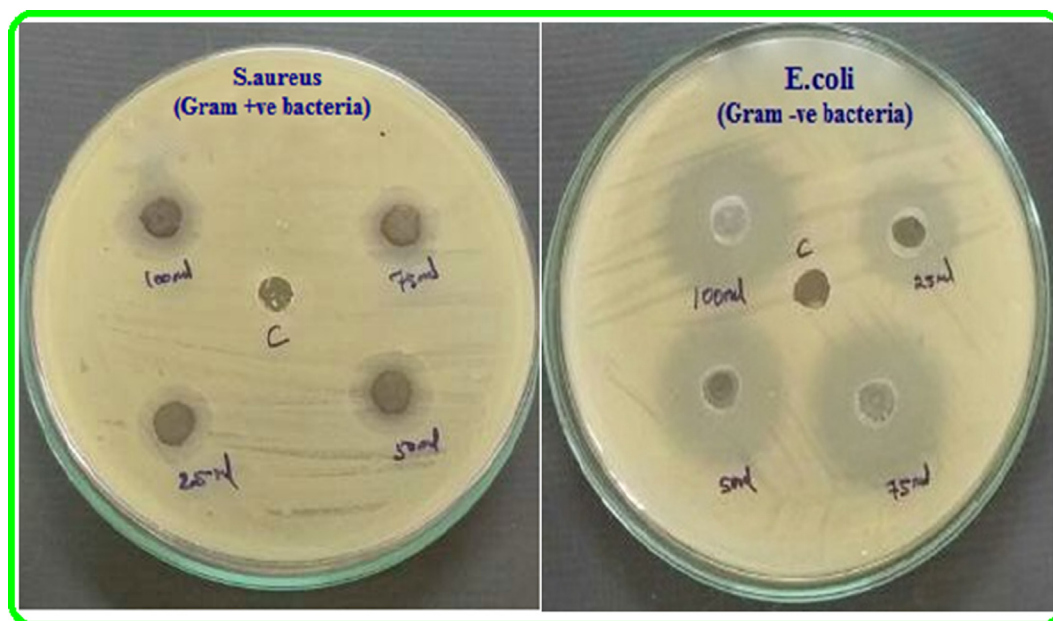

Fig. 8 Antibacterial activity of sample TNT/CS-CA@ M-HAP (II) coated on Ti specimen against gram positive and gram negative bacteria.

3.7. Apatite formation on the composite in SBF solution

Researchers have widely used SBF test to evaluate the capability of test samples to form an apatite layer on their surfaces. By performing SBF immersion, the apatite layer forming ability, or bioactivity of our TNT/CS-CA@M-HAP (II) nanocomposite can be assessed. The morphology of TNT/CS-CA@M-HAP (II) bioactive composite coatings were confirmed by the SBF immersion study for various days such as 1 day, 4 days, 7 days, 14 days and 21 days of immersion for the forming apatite layer are seen in SEM micrograph in the Fig. 9.

The apatite layer forming ability is major constituent mechanism of the chemical bioactivity. The growth of apatite on the nanocomposite coatings differ at each day. At day 1, there is no formation of apatite layer and after day 4, the started to grow on lesser number of apatite formation. At day 7, apatite


Fig. 7 Qualitative antibacterial activity of sample TNT/CS-CA@ M-HAP (II) coated on Ti specimen against gram positive and gram negative bacteria.

growth is seen on the surface of flower petal as displayed in Fig. 9c. At day 14, the growth of apatite was formed like spongy layer over the surfaces of nanocomposite coatings as shown in Fig. 9d. At day 21, some spongy flower like structure was observed as shown in Fig. 9e. In the sample, the formation of apatite layer usually takes place through an arrangement of chemical reactions. When coated samples were submerged in SBF solution, then the surface gains the positively charged ions that can attract negatively charged ions such as phosphate and hydroxyl group and forming Ca^{2+} poor amorphous in nature. This process indicates the formation of bone like apa-

tite growth on the nanocomposite surface (Alqarni et al., 2018). Thus, the HRSEM micrographs displayed the apatite mineralization ability at 7, 14 and 21 days of immersion and revealed that the resultant nanocomposite coatings improve the bioactivity in SBF solution.
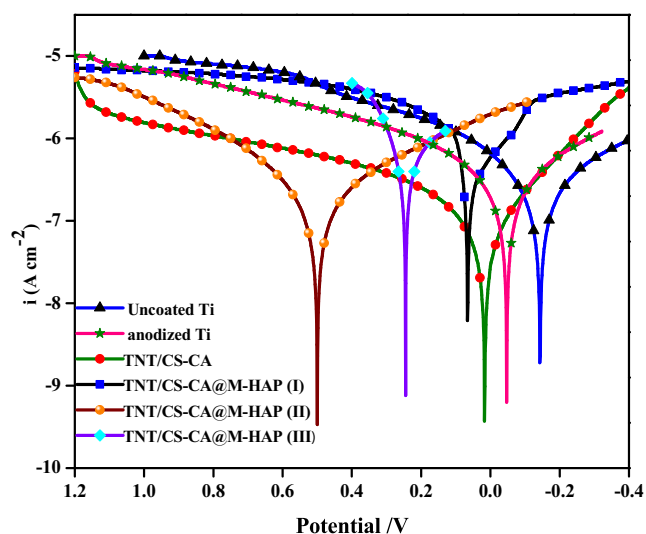
3.8. Electrochemical analysis

Electrochemical performances are one of the most universal tests to estimate the in vitro corrosion behavior of the formed
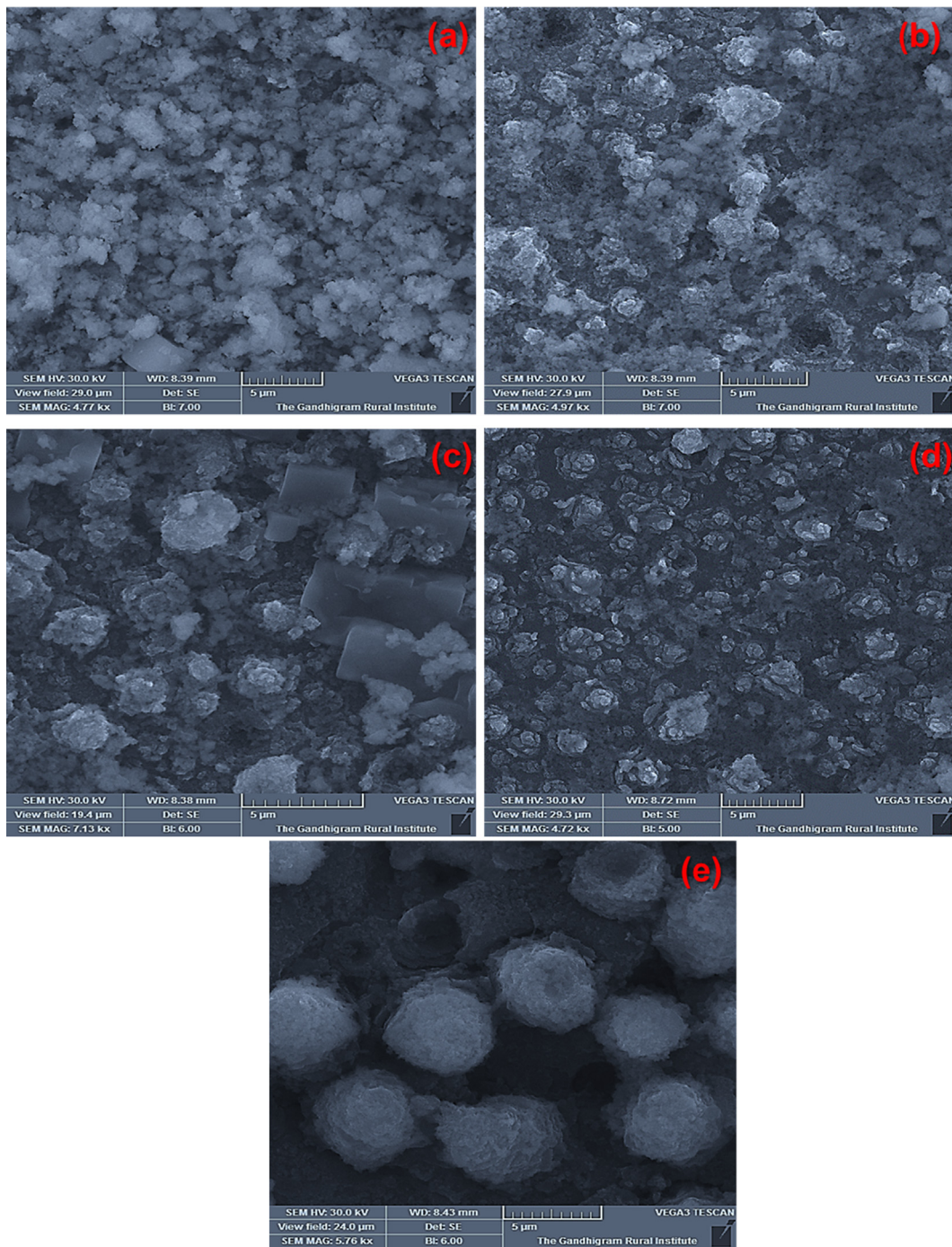
Fig. 9 HRSEM images of apatite formed on TNT/CS-CA@ M-HAP (II) bilayer coated on Ti samples dipped in SBF for several days (a) day 1, (b) day 4 (c) day 7 (d) day 14 and (e) day 21.

coatings, and it is generally composed of potentiodynamic polarization (Tafel exploitation plots) and Nyquist impedance plots. Fig. 10 displays the representative potentiodynamic polarization curves of the nanocomposite coatings of TNT/CS-CA and TNT/CS-CA@M-HAP, as well as TNT and uncoated Ti substrate in the Ringers physiological solution at 37 °C, and the related electrochemical parameters were determined from the polarization curves are summarized in Table 1. Potentiodynamic polarization measurements were done in the range from −0.4 V to 1.2 V vs. SCE, at a scan rate of 1.0 mV s^{-1} after reaching a steady state potential. The corrosion potential (E_{corr}, V), corrosion current density (i_{corr}, μA cm^{-2}), anodic as well as cathodic Tafel slopes (β_a, β_c) values were calculated at the points after E_{corr} values ± 100 mV using a computer least-squares method due to the degree of nonlinearity and eventually investigated uniform metal corrosion rate through Faraday's law (Fekry, 2016). The values of E_{corr} for tested six samples revealed a shift towards more positive values as obtained from the open circuit potential in the following order: TNT/CS-CA@M-HAP-II (0.501 V) > TNT/CS-CA@M-HAP-III (0.242 V) > TNT/CS-CA@M-HAP-I (0.059 V) > TNT/CS-CA (0.011 V) > TNT (-0.046 V) > uncoated Ti (-0.142 V). Also, the I_{corr} values increased in the same order, indicating that the TNT/CS-CA@M-HAP-II nanocomposite coating has the lowest I_{corr} value (0.61 A cm^{-2}) and compared to the uncoated Ti electrode which has the highest I_{corr} value (10 A cm^{-2}) with highest corrosion rate. However, M-HAP has decreased corrosion rate as the macromolecule is adsorbed well on the surface through electron pairs (Liu et al., 2017). When chitosan-casein polymer blended into TNT decreases the corrosion rate by increasing the film strength and then adding M-HAP into Chi-CA/TNT gives the lowest corrosion rate. This is due to minerals substituted HAP increasing the adsorption of both Chi-CA and Titania nanotubes to the Ti surface. The TNT increases the adhesion strength between the polymers and M-HAP composite matrix and the Ti surface. This leads to an increase in film stability, strength and adsorption

Table 1 Electrochemical parameters of uncoated Ti, Anodized Ti, TNT/CS-CA, TNT/CS-CA@M-HAP (I), TNT/CS-CA@M-HAP (II) and TNT/CS-CA@M-HAP (III) coated on Ti substrate.

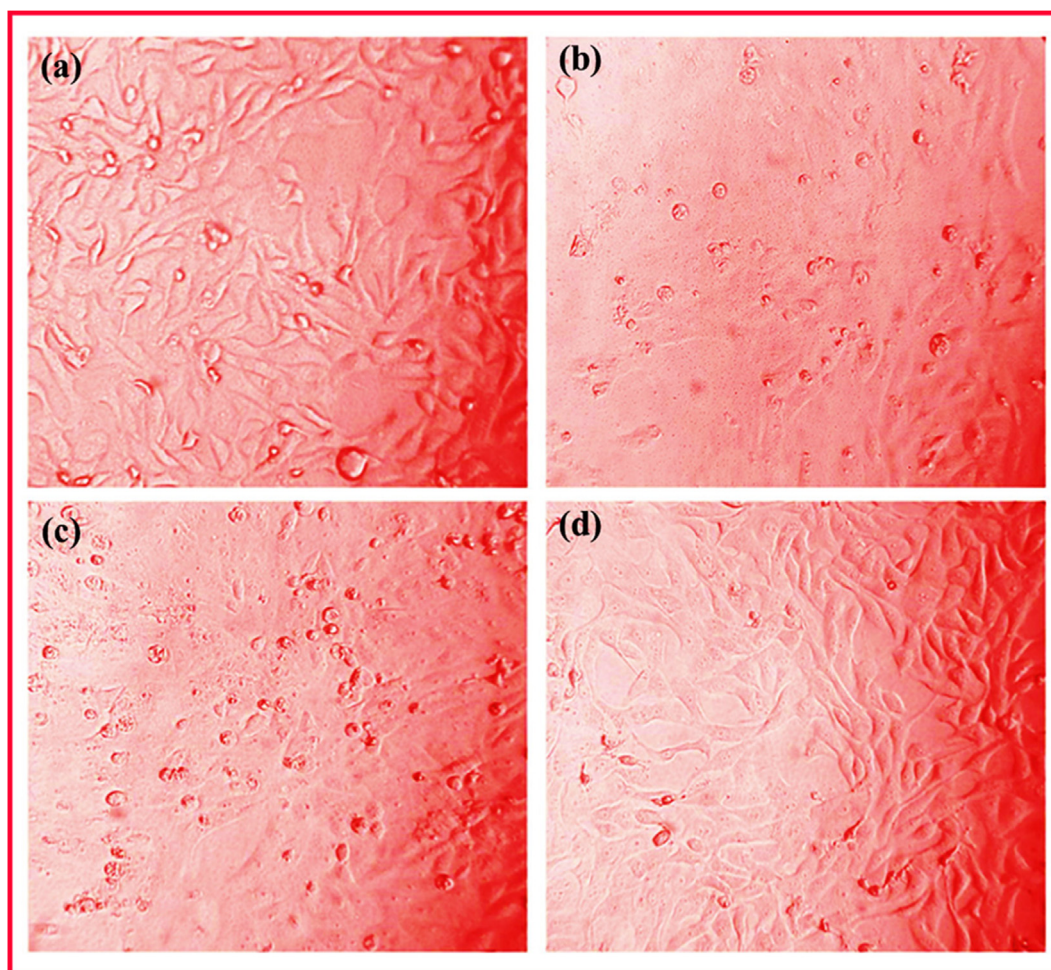| Samples	E_{corr}	Icorr × 10^{-7} (A cm^{-2})	Rct (Ω cm^2)
Uncoated Ti	−0.142	10.0	390
Anodized Ti	−0.046	7.9	624
TNT/CS-CA	0.011	1.8	726
TNT/CS-CA@M-HAP (I)	0.059	1.1	775
TNT/CS-CA@M-HAP (II)	**0.501**	**0.61**	**925**
TNT/CS-CA@M-HAP (III)	0.242	1.0	845
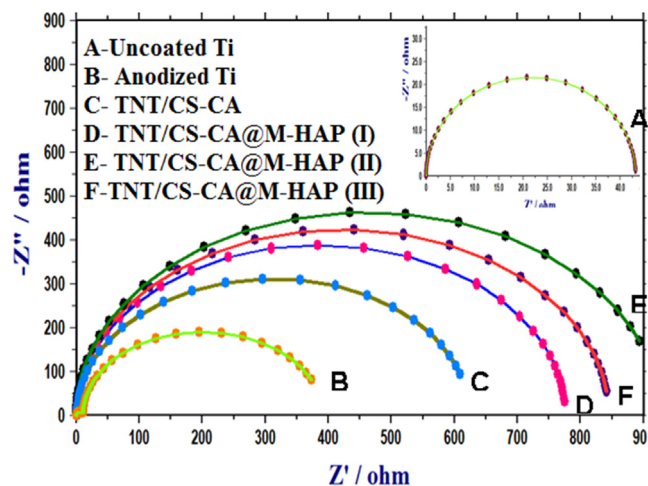
Fig. 11 Nyquist plots of uncoated Ti, anodized Ti, TNT/CS-CA and TNT/CS-CA@M-HAP (I) to TNT/CS-CA@M-HAP (III) coatings on Ti samples obtained in Ringer's solution.

on the Ti surface. Also, phosphate buffer solution forming ions helps in decreasing the lower corrosion rate of the Ti surface.

Finally, the M-HAP@Chi-CA/TNT nanostructured dense coating acts as a barrier to the transport of electrons and ions between the Ti alloy and the PBS solution. So, this novel synthesized nanocomposite coating significantly improved the corrosion resistance of the Ti alloy. Finally, the results of polarization curves are in the same trend with more positive corrosion potential compared to uncoated Ti surface (Li et al., 2014).

EIS results can give valuable information about the electrochemical behavior of both uncoated and coated Ti substrates in PBS solution. The impedance parameters derived from these plots using the equivalent electrical circuit are displayed in Fig. 11 and Table-1. The best circuit model was used to fit the EIS data for the corrosion behavior of uncoated and coated Ti substrates that consists of solution resistance (R_s), polarization resistance (R_p), charge transfer resistance of the coated substrate (R_{ct}) and double layer capacitance (C_{dl}).

Besides Bode and phase angle plots were also used to analyze the corrosion process. The high impedance modulus in lower frequency region and one time constant revealed that

Fig. 10 Potentiodynamic polarization curves of uncoated Ti, anodized Ti, TNT/CS-CA and TNT/CS-CA@M-HAP (I) to TNT/CS-CA@M-HAP (III) coatings on Ti samples obtained in Ringer's solution.

Fig. 12 Optical images showing the cell viability of MG63 human osteoblast cells on TNT/CS-CA@M-HAP (II) coatings for (a) 1, (b) 4 days and (c) 7 days of incubation.

the film has effective barrier property. In phase angle plots, TNT/CS-CA@M-HAP-II coating has higher phase angle and low frequency impedance modulus indicate the better corrosion resistance and passivity of stable structure are shown in Fig. S2(i, ii). At the same time, it is believed that the coated samples have higher phase angle and better corrosion resistance when compared to uncoated Ti surface. Because it has inert and homogenous film deposition on the surface.

3.9. Cell viability

The *in vitro* biocompatibility of cells over the TNT/CS-CA@M-HAP-II as-synthesized composite coatings is one of the most significant factors to assess the biological performance of the coating. The cell viability of MG 63 human osteoblast cells on TNT/CS-CA@M-HAP-II coatings was determined using an MTT assay for 1, 4 and 7 days of culture as shown in Fig.14. After the 24 h of incubation period, MTT solution (20 μL of 5 mg/ml serum free DMEM medium) was added into each well and the cells were incubated for another 2–4 h at 37 °C in a humidified 5% CO_2 atmosphere. The percentage of cell viability of various coatings is displayed as bar diagram in Fig. S3.

The absorbance of cell viability at a wavelength of 570 nm is directly proportional to the number of live cells in the present of MG63 human osteoblast cells culture medium are shown in Fig. S4. The optical images of the number of viable cells is increased as increasing after 7 days of incubation time as displayed in Fig. 12 (a-c). The MG63 cells were started to spread on the control over the surface on day 1. When compared to control at day 4, the cells were spread well through cytoskeletal processes over the composite coating. The TNT/CS-CA@M-HAP-II composite coatings exhibited more number of viable cells at day 7 compared with control as illustrated in the Fig. 14d, that does not display any toxicity of cells and also has good cytocompatibility. The cell viability results revealed that the as-developed coating can be served as a bio implant for orthopedic applications.

3.10. Live/dead staining

Fig. 13(a–d) shows the results of live/dead cells on the TNT/CS-CA@M-HAP-II nanocomposite coating at various days of incubation as determined by fluorescent microscopy.

The fluorescent microscopic images (Fig. 13a–d) denote the both live and dead stains indicating the green and red color.
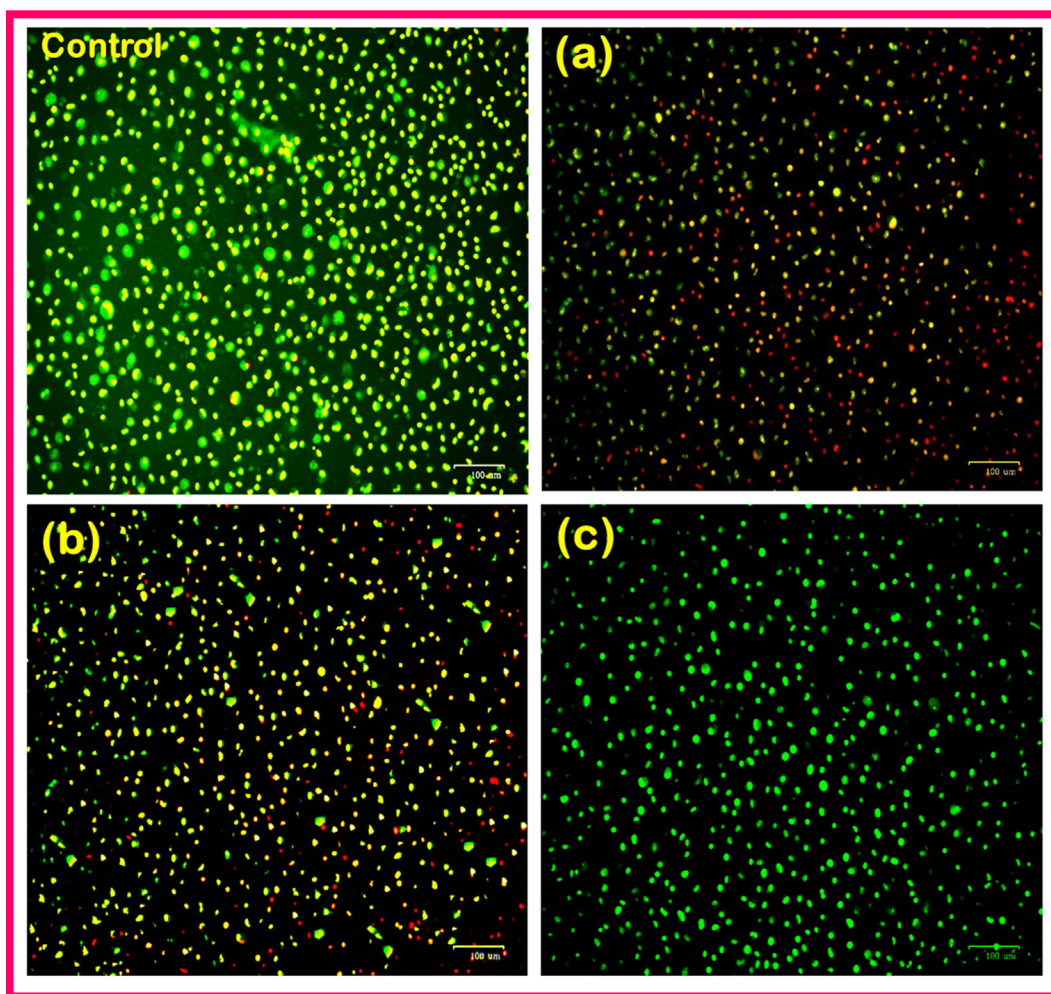
Fig. 13 Fluorescence microscopic images showing Live/dead staining MG63 human osteoblast cells on TNT/CS-CA@M-HAP (II) coatings for (a) control, (b) 1, (c) 4 days and (d) 7 days.

The evaluation of live/dead cells was carried out by culturing in medium for 1, 4 and 7 days. Fig. 13b indicated that the lesser number of live cells and more number of dead cells were spread well on the surface of TNT/CS-CA@M-HAP-II, respectively for 1 day of incubation when compared with control. The cells are spreading and growth with highly elongated morphology on TNT/CS-CA@M-HAP-II coated samples for 4 days of incubation as shown in fluorescent images in the Fig. 13c (Favi et al., 2013), (sathishkumar et al., 2016) (Li et al., 2014). The growth of MG 63 human osteoblast cells clearly exhibits that the cell proliferation on the TNT/CS-CA@M-HAP-II nanocomposite coated samples are well distributed throughout the surface of the coated material at higher absorbance of 7 days of incubation in cell culture (Fig. 13d), which is mainly due to the presence of mineral ions and polymer in the nanocomposite.

4. Conclusions

In this work, we reported a novel bioactive TNT/CS-CA@M-HAP-II nanocomposite coating material for orthopedic implants fabricated by anodization and electrodeposition methods. The structural morphology of the resultant coating was confirmed by the FT-IR, XRD and SEM with EDAX studies. From FESEM analysis, it is clearly shown that uniform and homogeneous TNT/CS-CA@M-HAP-II composite coatings were successfully fabricated onto the Ti specimen via the electrodeposition method. The electrochemical characterization confirmed the enhanced corrosion protection performance of TNT/CS-CA@M-HAP-II nanocomposite coating as it has lower current density and higher corrosion potential than other coatings in Ringer's solution. Thus, the results of antibacterial activity and cell viability studies revealed that TNT/CS-CA@M-HAP-II coating facilitates excellent antibacterial property and bone-like apatite formation. The cell viability and live/dead staining of MG-63 human osteoblast cells on the resultant nanocomposite coating provides better biocompatibility and bioactivity at immersion for 7 days. Hence, the TNT/CS-CA@M-HAP-II coating can be potential alternative bio implant material with good osseointegration for biomedical applications.

Declaration of Competing Interest

Acknowledgement

Appendix A. Supplementary material

Supplementary data to this article can be found online at https://doi.org/10.1016/j.arabjc.2020.05.031.

References

Abdul Manab, 2017. Casein polysaccaharides interaction – a review. Int. J. ChemTech. Res. 10, 01–09.

Agarwal, S., Curtin, J., Duffy, B., Jaiswal, S., 2016. Biodegradable magnesium alloys for orthopaedic applications: a review on corrosion, biocompatibility and surface modifications. Mater. Sci. Eng., C 68, 948–963. https://doi.org/10.1016/j.msec.2016.06.020.

Alqarni, N.D., Wysocka, J., El-Bagoury, N., Ryl, J., Amin, M.A., Boukherroub, R., 2018. Effect of cobalt addition on the corrosion behavior of near equiatomic NiTi shape memory alloy in normal saline solution: electrochemical and XPS studies. RSC Adv. 8, 19289–19300. https://doi.org/10.1039/c8ra02031k.

Azhar, F.F., Olad, A., Salehi, R., 2014. Fabrication and characterization of chitosan–gelatin/nanohydroxyapatite–polyaniline composite with potential application in tissue engineering scaffolds. Des. Monomers Polym. 17 (7), 654–667.

Bai, L., Zhang, J., Weng, Z., Liu, S., Zhao, Y., Liu, Y., Zhang, X., Huang, X., Yao, X., Hang, R., Tang, B., Du, Z., Crawford, R., Xiao, Y., Du, J., Huang, D., Yao, W., 2018. A multifaceted coating on titanium dictates osteoimmunomodulation and osteo/angiogenesis towards ameliorative osseointegration. Biomaterials 162, 154–169. https://doi.org/10.1016/j.biomaterials.2018.02.010.

Biranje, S., Madiwale, P., Adivarekar, R.V., 2019. Porous electrospun Casein/PVA nanofibrous mat for its potential application as wound dressing material. J. Porous Mater. 26, 29–40. https://doi.org/10.1007/s10934-018-0602-7.

Chang, L., Sun, J., Fuh, J.Y.H., Thian, E.S., 2013. Deposition and characterization of a dual-layer silicon- and silver-containing hydroxyapatite coating via a drop-on-demand technique. RSC Adv. 3, 11162–11168. https://doi.org/10.1039/c3ra23251d.

Chen, X., Jin, X., Tan, J., Li, W., Chen, M., Yao, L., Yang, H., 2016. Large-scale synthesis of water-soluble luminescent hydroxyapatite nanorods for security printing. J. Colloid Interface Sci. https://doi.org/10.1016/j.jcis.2016.01.078.

Civantos, A., Campos, E.M., Ramos, V., Elvira, C., Gallardo, A., Abarrategi, A., 2017. Titanium coatings and surface modifications: toward clinically useful bioactive implants. ACS Biomater. Sci. Eng. 3, 1245–1261.

Das, G.K., Heng, B.C., Ng, S.C., White, T., Loo, J.S.C., D'Silva, L., Padmanabhan, P., Bhakoo, K., Selvan, S.T., Tan, T.T.Y., 2010. Gadolinium oxide ultranarrow nanorods as multimodal contrast agents for optical and magnetic resonance imaging. Langmuir 26, 8959–8965.

Devi, N., Sarmah, M., Khatun, B., Maji, T.K., 2016. Encapsulation of active ingredients in polysaccharide-protein complex coacervates.

Adv. Colloid Interface Sci. https://doi.org/10.1016/j.cis.2016.05.009.

Farzadi, A., Bakhshi, F., Solati-Hashjin, M., Asadi-Eydivand, M., Osman, N.A.A., 2014. Magnesium incorporated hydroxyapatite: Synthesis and structural properties characterization. Ceram. Int. 40, 6021–6029. https://doi.org/10.1016/j.ceramint.2013.11.051.

Favi, P.M., Benson, R.S., Neilsen, N.R., Hammonds, R.L., Bates, C. C., Stephens, C.P., Dhar, M.S., 2013. Cell proliferation, viability, and in vitro differentiation of equine mesenchymal stem cells seeded on bacterial cellulose hydrogel scaffolds. Mater. Sci. Eng., C 33, 1935–1944. https://doi.org/10.1016/j.msec.2012.12.100.

Fekry, A.M., 2016. Electrochemical behavior of a novel nano-composite coat on Ti alloy in phosphate buffer solution for biomedical applications. RSC Adv. 6, 20276–20285. https://doi.org/10.1039/c6ra01064d.

Govindaraj, D., Rajan, M., Munusamy, M.A., Higuchi, A., 2015. Mineral substituted hydroxyapatite coatings deposited on nanoporous TiO2 modulate the directional growth and activity of osteoblastic cells. RSC Adv. 5, 58980–58988. https://doi.org/10.1039/c5ra11037h.

Hamedi, M., Wigenius, J., Tai, F., Björk, P., Aili, D., 2010. Linköping University Post Print Polypeptide-guided assembly of conducting polymer nanocomposites Polypeptide-Guided Assembly of Conducting Polymer Nanocomposites 2058–2061. https://doi.org/10.1039/b000000x.

Hosseini, S.M., Drouet, C., Al-Kattan, A., Navrotsky, A., 2014. Energetics of lanthanide-doped calcium phosphate apatite. Am. Mineral. 99, 2320–2327. https://doi.org/10.2138/am-2014-4930.

Jadalannagari, S., Deshmukh, K., Verma, A.K., Vohra, R., Kowshik, M., Ramanan, S.R., 2014. Lanthanum-doped hydroxyapatite nanoparticles as biocompatible fluorescent probes for cellular internalization and biolabeling. Sci. Adv. Mater. 6, 1–8.

Kolanthai, E., Colon, V.S.D., Sindu, P.A., 2015. Effect of solvent; Enhancing the wettability and engineering the porous structure of a calcium phosphate/agarose composite for drug delivery. RSC Adv. 5, 18301–18311.

Kumar, A.M., Kwon, S.H., Jung, H.C., Park, Y.H., Kim, H.J., Shin, K.S., 2014. Fabrication and electrochemical corrosion behavior of PEO coatings on strip-cast AZ31Mg alloy in 3.5% NaCl solution. Ind. Eng. Chem. Res. 53, 9703–9713.

Kurek, M., Galus, S., Debeaufort, F., 2014. Surface, mechanical and barrier properties of bio-based composite films based on chitosan and whey protein. Food Packag. Shelf Life 1, 56–67. https://doi.org/10.1016/j.fpsl.2014.01.001.

Lee, B.G., Choi, J.W., Lee, S.E., Jeong, Y.S., Oh, H.J., Chi, C.S., 2009. Formation behavior of anodic TiO$_2$ nanotubes in fluoride containing electrolytes. Trans. Nonferrous Met. Soc. China 19, 842–845 (English Edition).

Lotz, E.M., Berger, M.B., Schwartz, Z., Boyan, B.D., 2018. Regulation of osteoclasts by osteoblast lineage cells depends on titanium implant surface properties. Acta Biomater. 68, 296–307. https://doi.org/10.1016/j.actbio.2017.12.039.

Li, B., Han, Y., Qi, K., 2014. Formation mechanism, degradation behavior, and cytocompatibility of a nanorod-shaped HA and pore-sealed MgO bilayer coating on magnesium. ACS Appl. Mater. Interfaces 6, 18258–18274. https://doi.org/10.1021/am505437e.

Liu, J., Lou, Y., Zhang, C., Yin, S., Li, H., Sun, D., Sun, X., 2017. Improved corrosion resistance and antibacterial properties of composite arch-wires by N-doped TiO$_2$ coating. RSC Adv. 7, 43938–43949. https://doi.org/10.1039/c7ra06960j.

Metoki, N., Liu, L., Beilis, E., Eliaz, N., Mandler, D., 2014. Preparation and characterization of alkylphosphonic acid self-assembled monolayers on titanium alloy by chemisorption and electrochemical deposition. Langmuir 30, 6791–6799. https://doi.org/10.1021/la404829b.

Mohan Raj, R., Priya, P., Raj, V., 2018. Gentamicin-loaded ceramic-biopolymer dual layer coatings on the Ti with improved bioactive

and corrosion resistance properties for orthopedic applications. J. Mech. Behav. Biomed. Mater. 82, 299–309.

Pishbin, F., Kreppel, S., Ryan, M.P., Boccaccini, A.R., Mouriño, V., Flor, S., Salih, V., 2014. Electrophoretic deposition of gentamicin-loaded bioactive glass/chitosan composite coatings for orthopaedic implants. ACS Appl. Mater. Interfaces 6, 8796–8806. https://doi.org/10.1021/am5014166.

Pogrebjak, A.D., Krivets, A.S., Dyadyura, K.A., Maksakova, O.V., Shaimardanov, Zh.K., Peplinska, B. 2016. Research of the relief and element composition of the surface coatings based on hydroxyapatite implants from titanium alloys. In: Proceedings of the 6th International Conference Nanomaterials: Applications and Properties, NAP 2016. SEP 14-19 (2016) UNSP 02NABM06.

Pogrebnjak, A.D., Kong, C.H., Webster, R.F., Tilley, R.D., Takeda, Y., Oyoshi, K., Bondar, O.V., Buranich, V.V., Konstantinov, S.V., Baimoldanova, L.S., Opielak, M., Zukowski, P., Konarski, P., 2019. Antibacterial effect of Au implantation in ductile nanocomposite multilayer (TiAlSiY)N/CrN Coatings. ACS Appl. Mater. Interfaces 11, 48540–48550.

Poverenov, E., Rutenberg, R., Danino, S., Horev, B., Rodov, V., 2014. Gelatin-chitosan composite films and edible coatings to enhance the quality of food products: layer-by-layer vs blended formulations. Food Bioprocess Technol. 7, 3319–3327. https://doi.org/10.1007/s11947-014-1333-7.

Qin, L., Dong, H., Mu, Z., Zhang, Y., Dong, G., 2015. Preparation and bioactive properties of chitosan and casein phosphopeptides composite coatings for orthopedic implants. Carbohydr. Polym. 133, 236–244. https://doi.org/10.1016/j.carbpol.2015.06.099.

Raj, V., Mohan Raj, R., 2016. Fabrication of TiO$_2$-strontium loaded CaSiO$_3$/biopolymer coatings with enhanced biocompatibility and corrosion resistance by controlled release of minerals for improved orthopaedic applications. J. Mech. Behav. Biomed. Mater. 60, 476–491. https://doi.org/10.1016/j.jmbbm.2016.02.021.

Sasireka, A., Rajendran, R., Priya, P., Raj, V., 2019. Ciprofloxacin-loaded ceramic/polymer composite coatings on Ti with improved antibacterial and corrosion resistance properties for orthopedic applications. ChemistrySelect 4, 1166–1175. https://doi.org/10.1002/slct.201803769.

Sathishkumar, S., Louis, K., Shinyjoy, E., Gopi, D., 2016. Tailoring the Sm/Gd substituted hydroxyapatite coating on biomedical AISI 316L SS: Exploration of corrosion resistance, protein profiling, osteocompatibility and osteogenic differentiation for orthopedic implant applications. Ind. Eng. Chem. Res. https://doi.org/10.1021/acs.iecr.5b04329.

Saini, M., 2015. Implant biomaterials: a comprehensive review. World J. Clin. Cases 3, 52 https://doi.org/10.12998/wjcc.v3.i1.52.

Singh, A., Bajpai, J., Tiwari, A., Bajpai, A.K., 2015. Designing casein-coated iron oxide nanostructures (CCIONPs) as super-paramagnetic core–shell carriers for magnetic drug targeting. Prog. Biomater. 4, 39–53. https://doi.org/10.1007/s40204-014-0035-6.

Sohn, Y., 2014. Structural and spectroscopic characteristics of terbium hydroxide/oxide nanorods and plates. Ceram. Int. 40 (9), 13803–13811. https://doi.org/10.1016/j.ceramint.2014.05.096.

Stancheva, M., Bojinov, M., 2012. Influence of fluoride content on the barrier layer formation and titanium dissolution in ethylene glycol-water electrolytes. Electrochim. Acta 78, 65–74. https://doi.org/10.1016/j.electacta.2012.05.093.

Surmeneva, M.A., Kovtun, A., Peetsch, A., Goroja, S.N., Sharonova, A.A., Pichugin, V.F., Grubova, I.Y., Ivanova, A.A., Teresov, A.D., Koval, N.N., Buck, V., Wittmar, A., Ulbricht, M., Prymak, O., Epple, M., Surmenev, R.A., 2013. Preparation of a silicate-containing hydroxyapatite-based coating by magnetron sputtering: Structure and osteoblast-like MG63 cells in vitro study. RSC Adv. 3, 11240–11246. https://doi.org/10.1039/c3ra40446c.